Title: Studies of dynamics of a lightweight wheeled mobile robot during longitudinal motion on soft ground

Author: Maciej Trojnacki Przemysław Dąbek

PII: S0093-6413(16)30285-3
DOI: http://dx.doi.org/doi:10.1016/j.mechrescom.2016.11.001
Reference: MRC 3125

To appear in:

Received date: 15-4-2016
Revised date: 2-11-2016
Accepted date: 7-11-2016

Please cite this article as: Trojnacki, Maciej, Dąbek, Przemysław, Studies of dynamics of a lightweight wheeled mobile robot during longitudinal motion on soft ground.Mechanics Research Communications http://dx.doi.org/10.1016/j.mechrescom.2016.11.001

Studies of dynamics of a lightweight wheeled mobile robot during longitudinal motion on soft ground

Maciej TROJNACKI, Przemysław DĄBEK

Industrial Research Institute for Automation and Measurements (PIAP), Al. Jerozolimskie 202, 02-486 Warsaw, Poland

*mtrojnacki@piap.pl; *pdabek@piap.pl*
Tel.:+48-87-40-164; fax: +48-87-40-221
Accepted: April 15, 2013.

Highlights

1. Influence of desired velocity on selected robot motion parameters is investigated.
2. Empirical studies are conducted in the container with dry sand.
3. Simulations are based on multi-body method and classical terramechanics models.
4. Formula for front-to-back contact angle ratio dependency on velocity is proposed.

Abstract

The paper is concerned with the study of longitudinal motion of a lightweight wheeled mobile robot on soft ground. The study is focused on the influence of the desired longitudinal velocity of a robot on both the longitudinal slip of the wheels and the ratio of wheel-terrain contact angles. Design of the four-wheeled skid-steered robot and research environment are described. Experimental investigations were conducted on a dedicated test stand with dry sand. A dynamics model of the robot-ground system taking into account properties of soft ground is presented. The classical terramechanics models of Bekker and Janosi-Hanamoto are used. Results of simulation research of robot motion and of the analogous experimental investigations are presented. Actual motion parameters of the robot and the values of longitudinal slip ratio of the wheels are determined. The results of simulation and experimental investigations are compared and discussed. A formula to describe front-to-back wheel-terrain contact angle ratio dependency on the desired velocity is proposed.

Keywords: wheeled mobile robot, soft ground, tire-ground model, longitudinal velocity, wheel slip

1. Introduction

Wheeled mobile robots are unmanned vehicles whose motion is primarily a result of interaction of the wheels with the ground. In the case of robot motion on the soft ground, wheel slip phenomena and ground deformability should be considered in the model of robot dynamics. The dynamics model can be used, among other applications, as a tool in the process of robot mechatronic design.

The problems of modeling of the tire-ground system were considered so far mainly from the point of view of requirements of automotive vehicles, which over the years resulted in the development of multiple tire models with diverse capabilities, both on-road [1] and off-road [2,3]. However, it turns out that the wheeled mobile robots, especially lightweight robots, differ significantly from automotive vehicles in terms of applications, maneuvers performed, types of ground on which they move, vehicle design and properties of tires [4]. It seems that there is much less work done so far in the field of modeling of tire-road interaction for medium-weight and lightweight wheeled robots. Most studies are concerned with wheel-terrain interaction of planetary rovers, for instance [5–8].

One of the questions, important from the point of view of robot mobility and efficiency of motion, is the influence of the robot desired velocity. Some studies focus on the influence of wheel slip on vehicle mobility [8] and efficiency [9], but not many on the influence of desired vehicle velocity on wheel slip.

The aim of the present work is a numerical and experimental study of the dynamics of a lightweight skid-steered wheeled mobile robot on deformable ground with a focus on the desired velocity influence on robot motion parameters, especially on wheel slip. An important feature of the study is that the robot is equipped with non-pneumatic tires of small diameter. Results of

the study are then used to enhance the multi-body model of robot dynamics based on the classical terramechanics models of Bekker and Janosi-Hanamoto.

The present article is an extended version of the conference paper [10], which concentrated on the phase of robot motion with constant desired velocity (excluding speeding up and braking phases). For this case, on the basis of experimental investigations, relationships between robot velocity and slip ratio and between robot velocity and the ratio of angles of wheel-terrain contact in front and rear parts of the wheel were proposed. In the current work the relationship between the ratio of contact angles and velocity is implemented in the robot dynamics model. This enables changes of this ratio during robot acceleration and braking phases to be included in the simulations. Moreover, the multi-body dynamics model of the robot is improved by taking into account small difference between components of the ground reaction forces in robot and ground coordinate systems resulting from the variable pitch angle of robot body. Both mentioned improvements in the model yielded a new version of simulation results in comparison to [10]. In the present work the results of simulation and experimental research for the desired velocities of robot motion are limited to the range of 0.2-0.7 m/s (1 m/s case excluded), because in this range a particularly good agreement of experimental and simulation results was obtained.

2. Four-wheeled skid-steered mobile robot

The object of the research is a small four-wheeled mobile robot called PIAP GRANITE (Ground Robot for ANalyzes of wheels Interaction with various TErrain). The robot has all wheels driven independently by DC servomotors with gear units and encoders. The kinematic structure of the robot is shown in Fig. 1a.

It is possible to distinguish the following main components of the robot: 0 – body with frame for installation of the research equipment, 1-4 – wheels with toothed belt pulleys, 5-6 – toothed belts. The drive transmission in each drive unit can be decoupled and also the toothed belts can be removed which permits obtaining various configurations of the robot drive system. In the present paper, configuration of the robot with independent driving of all four wheels and without the toothed belts is analyzed.

The following symbols for the i^{th} wheel have been introduced in the robot model: A_i – geometrical center, $r_i = r$ – radius, $b_i = b$ – width of tire tread, θ_i – angle of wheel spin (i = 1,..., 4).

The robot in the present work is equipped with a laptop computer and inertial measurement units. Motion parameters of the robot can be determined according to the method proposed in [11]. Moreover, dual tires are used so that the clearance between ground surface and bottom of the robot body can be preserved during motion on soft ground like sand.

3. Modeling of the robot and tire-ground interaction

3.1. Robot kinematics

In this paper the longitudinal motion of the robot is analyzed. It is assumed that this motion takes place in *Oxz* plane of the fixed coordinate system $\{O\}$. The moving coordinate system associated with the robot is denoted with symbol $\{R\}$.

In the considered case, the desired parameter of robot motion will be velocity of the characteristic point R of the robot (Fig. 1a), that is ${}^{O}v_{Rd}$. Because the robot is in longitudinal motion, velocities of geometric centers of wheels, that is ${}^{O}v_{Ai}$, should be equal to ${}^{O}v_{Rd}$ velocity. In practice, during robot motion wheel slips occur. The measure of instantaneous longitudinal wheel slip is the (longitudinal) slip ratio, which can be calculated from the following formula based on [3]:

$$\lambda_i = \begin{cases} 0 \quad \text{for} \quad v_{oi} = 0, \\ (v_{oi} - {}^{R}v_{Aix}) / \max(v_{oi},\ {}^{R}v_{Aix}) \quad \text{for other} \quad v_{oi}, \end{cases} \tag{1}$$

where $v_{oi} = \dot{\theta}_i r_i$ and ${}^{R}v_{Aix}$ are respectively velocity at the wheel circumference and longitudinal component of velocity of the wheel geometric center for the i^{th} wheel.

Another measure of the longitudinal slip of the wheel, this time for the robot locomotion system considered as a whole, can be the robot longitudinal slip ratio in the form:

$$\lambda_R = (s_{Rxd} - s_{Rx}) / s_{Rxd}, \tag{2}$$

where: s_{Rx} – actual distance traversed by a robot in longitudinal direction, s_{Rxd} – desired distance, equivalent to the distance traversed in the case of wheel rolling without slip.

This kind of longitudinal slip measure can be used especially in the case of robots moving with small velocities like planetary rovers. This measure can be also used for larger velocities of motion, on condition that only the part of trajectory when the robot is in steady motion will be taken into account.

3.2. Tire-terrain interaction model

Modeling assumptions. As far as conditions of wheel-deformable ground interaction are concerned, in the model the following aspects can be taken into account: the case of a stationary tire, different rut depth under and behind the tire,

deformability of tire, passage of trailing wheels in the rut made by the leading wheels (multi-pass) and the associated phenomenon of soil compaction, bulldozing effect in front of the tire, damping in the tire-ground system, and shape of the tire tread.

In the present work, during determination of the longitudinal slip, based on which the longitudinal wheel force is calculated, the case of a stationary wheel is included, which allows determination of forces and moments acting on the robot before motion begins and after it is finished. In the work, the phenomenon of slightly greater rut depth directly under the tire as compared to the place just behind the tire is also taken into account. It is assumed that the robot wheels are rigid bodies, which is the assumption frequently made by other authors in the case of vehicle motion on sand. In the tire-ground model the multi-pass effect is not included. This effect will occur in the case of longitudinal motion and will affect the results obtained from the simulation studies. However, this influence will be negligible if the soil was already compacted (subjected to pressure) before motion and it is frequently neglected in models. The tire-ground interaction damping is included, because otherwise the undamped oscillations would occur in the model. In the work the overall tread shape and shapes of individual tread blocks are not taken into account.

Tire and ground deformation. In Fig. 1b the wheel load is schematically illustrated for the case of rigid wheel. In the figure are shown: the driving moment for the wheel $\mathbf{T}_i$, the tangential $\boldsymbol{\tau}_i(\vartheta_i)$ and normal $\boldsymbol{\sigma}_i(\vartheta_i)$ stresses and the resultant pressure $\mathbf{p}_i(\vartheta_i)$ at a certain point of the wheel-ground contact, that is, for the angle ϑ_i, the angular velocity of wheel spin $\boldsymbol{\omega}_i$, the longitudinal velocity of geometric center of wheel ${}^R\mathbf{v}_{Aix}$, the characteristic angles ϑ_{1i}, ϑ_{2i} and maximum wheel sinkage z_{0i}.

While the ϑ_{1i} angle and the maximum ground deformation z_{0i} can be calculated from geometric relationships, the same is not possible for the ϑ_{2i} angle. In the case when the wheel is stationary, one may assume that the angle ϑ_{2i} is equal to the angle ϑ_{1i}. More difficult is, however, determination of the angle ϑ_{2i} during robot motion, and it has a visible influence on the value of the longitudinal force ${}^RF_{Aix}$.

In the literature sometimes the zero value of this angle is assumed, which may lead to an undervalued longitudinal force ${}^RF_{Aix}$ as compared to its experimental value. More often models with a certain small value of this angle relatively to the angle ϑ_{1i} can be found. In some works, like [13], the following equation is used:

$$\vartheta_{2i} = (b_0 + b_1 |\lambda_i|)\vartheta_{1i}, \tag{3}$$

where b_0 and b_1 are the soil dependent constants.

A drawback of the above relationship is that in the case of a robot standing still $\lambda_i = 0$ and $\vartheta_{1i} = \vartheta_{2i}$. Because $\lambda_i = 0$ can also occur during robot motion (especially during braking), based on the λ_i value alone it is not possible to uniquely determine the ϑ_{2i} angle value. Moreover, the expression in the parentheses should be non-negative, that is the minimum value of the ϑ_{2i} angle should be equal to 0.

In the present work, a different approach was adopted, that is, the angle ϑ_{2i} is calculated from the relationship:

$$\vartheta_{2i} = k_{\vartheta 2}({}^O v_{Rd})\vartheta_{1i}, \tag{4}$$

where the ratio $k_{\vartheta 2}$ will be a function of the desired robot velocity ${}^O v_{Rd}$ and the form of the function will be chosen as a result of a procedure of fitting the simulation results to the experimental results so as to obtain an adequate value of the longitudinal force ${}^RF_{Aix}$.

This ratio will be approximated by the function:

$$k_{\vartheta 2}({}^O v_{Rd}) = \exp(-a_\vartheta \, {}^O v_{Rd}), \tag{5}$$

with the assumption that in the case of the robot standing still $k_{\vartheta 2} = 1$, which follows from the fact that $\vartheta_{1i} = \vartheta_{2i}$.

To calculate the soil shear displacement in the range $\vartheta_i \in \langle -\vartheta_{2i}, \vartheta_{1i} \rangle$ the following formula will be used [12]:

$$j_i(\vartheta_i) = r_i\big((\vartheta_{1i} - \vartheta_i) - (1-\lambda_i)(\sin\vartheta_{1i} - \sin\vartheta_i)\big), \tag{6}$$

while the static sinkage will be calculated from the relationship:

$$z_i(\vartheta_i) = \max\big(z_{0i} - r_i(1-\cos\vartheta_i), 0\big). \tag{7}$$

Ground model and stress. During analysis of robot motion on a deformable ground like sand, model of the soil should be taken into account in which important are relations between the pressure and the sinkage as well as between the shear stress and the shear displacement. The pressure-sinkage relation can be described using Bekker formula [2]:

$$p_i(\vartheta_i) = k\left(z_i(\vartheta_i)\right)^n = \left(\frac{k_c}{b_i} + k_\phi\right)\left(z_i(\vartheta_i)\right)^n, \tag{8}$$

where: $p_i(\vartheta_i)$ – pressure, $z_i(\vartheta_i)$ – static sinkage, b_i – width of the tire tread, k_c – cohesive modulus of terrain deformation, k_ϕ – frictional modulus of terrain deformation, n – exponent of terrain deformation.

Usually the implicit assumption is made that the normal stresses $\sigma(\vartheta_i)$ acting on a tire at particular points have values close to $p(\vartheta_i)$, that is the following approximation holds true:

$$\sigma_i(\vartheta_i) \approx p_i(\vartheta_i). \tag{9}$$

This assumption is correct in the case of small angle $\delta_i(\vartheta_i)$ between directions of the pressure $p_i(\vartheta_i)$ and the stress $\sigma_i(\vartheta_i)$, and it allows to obtain the results of satisfactory accuracy.

The dependency between the maximum shear stress $\tau_{imax}(\vartheta_i)$ and the normal stress $\sigma_i(\vartheta_i)$ can be described by the Mohr-Coulomb failure criteria [2] also including the case of moving a tire surface with respect to soil, that is in the form [14]:

$$\tau_{imax}(\vartheta_i) = \min\left(\mu_s \sigma_i(\vartheta_i),\ c + \sigma_i(\vartheta_i)\tan\phi\right), \tag{10}$$

where: c – coefficient of cohesion of soil, ϕ – angle of internal friction, μ_s – tire-soil static friction coefficient, which for the rubber tire-dry sand is equal to $\mu_s = 0.6$ ([15]).

According to Janosi-Hanamoto hypothesis [3], the tangential stress is determined based on the relationship:

$$\tau_i(\vartheta_i) = \tau_{imax}(\vartheta_i)\left(1 - \exp\left(\frac{-j_i(\vartheta_i)}{K}\right)\right), \tag{11}$$

where: K – the shear deformation parameter.

The present work focuses on the investigations of the robot longitudinal motion on dry sand. The parameters of sand proposed in the work [8] will be used in further considerations (Tab. 1).

Forces and moments of force acting on the wheel from the ground. Based on the known tangential and normal stresses acting on the tire from the ground over the arc described by the angle $\vartheta_i \in \langle -\vartheta_{2i}, \vartheta_{1i} \rangle$ and treating the robot wheel as a rigid body, it is possible to calculate the resultant forces and moments of force acting on the wheel, that is, the static vertical load, the motion resistance force, the traction force and the wheel load torque using the respective formulas:

$$W_i = b_i r_i \int_{-\vartheta_{2i}}^{\vartheta_{1i}} w_i(\vartheta_i)\,\mathrm{d}\vartheta_i = b_i r_i \int_{-\vartheta_{2i}}^{\vartheta_{1i}} \left(\sigma_i(\vartheta_i)\cos\vartheta_i + \tau_i(\vartheta_i)\sin\vartheta_i\right)\mathrm{d}\vartheta_i, \tag{12}$$

$$R_{ti} = b_i r_i \int_{-\vartheta_{2i}}^{\vartheta_{1i}} r_{ti}(\vartheta_i)\,\mathrm{d}\vartheta_i = b_i r_i \int_{-\vartheta_{2i}}^{\vartheta_{1i}} \sigma_i(\vartheta_i)\sin\vartheta_i\,\mathrm{d}\vartheta_i, \tag{13}$$

$$F_i = b_i r_i \int_{-\vartheta_{2i}}^{\vartheta_{1i}} f_i(\vartheta_i)\,\mathrm{d}\vartheta_i = b_i r_i \int_{-\vartheta_{2i}}^{\vartheta_{1i}} \tau_i(\vartheta_i)\cos\vartheta_i\,\mathrm{d}\vartheta_i, \tag{14}$$

$$M_{\omega i} = -b_i (r_i)^2 \int_{-\vartheta_{2i}}^{\vartheta_{1i}} \tau_i(\vartheta_i)\,\mathrm{d}\vartheta_i. \tag{15}$$

The longitudinal force ${}^{O}F_{Tix}$ acting on the tire is the resultant of the motion resistance and the traction force:

$${}^{O}F_{Tix} = F_i + R_{ti}. \tag{16}$$

The normal force ${}^{O}F_{Tiz}$ acting on the tire should be determined based on the static vertical load after including the damping of tire-ground system, i.e. from the relationship:

$${}^{O}F_{Tiz} = W_i + c_{ti}\,\dot{z}_{0i}\,\mathrm{sgn}(z_{0i}), \tag{17}$$

where c_{ti} is the damping coefficient for the tire-ground system.

Eventually, the forces and moments of force acting on particular wheels can be reduced to the wheel geometric centers and written in the following vector form:

$${}^{O}\mathbf{F}_{Ai} = [{}^{O}F_{Aix},\, 0,\, {}^{O}F_{Aiz}]^T = [{}^{O}F_{Tix},\, 0,\, {}^{O}F_{Tiz}]^T, \quad {}^{O}\mathbf{M}_{Ai} = [0,\, M_{\omega i},\, 0]^T. \tag{18}$$

3.3. Multi-body dynamics model

In the present work the dynamics model of PIAP GRANITE robot will be introduced for the case of longitudinal motion on a horizontal ground.

It is assumed that the robot is under action of the following external forces: the ground reaction forces acting on each wheel ${}^{O}\mathbf{F}_{Ti} = [{}^{O}F_{Tix}, {}^{O}F_{Tiy}, {}^{O}F_{Tiz}]^T$ (i = 1, ..., 4), the gravity force ${}^{O}\mathbf{G} = m_R\,{}^{O}\mathbf{g}$, where m_R denotes the total mass of the robot. The mentioned forces acting on the robot and on the wheel are illustrated in Fig. 2. The particular pairs of wheels are additionally denoted with the subscripts: f – the front wheels (f = 1, 2), b – the back wheels (b = 3, 4).

The gravity force vector ${}^{O}\mathbf{G}$ is a function of a gravitational acceleration vector ${}^{O}\mathbf{g} = [0,\, 0,\, -g]^T$, where $g = 9.81$ m/s^2 is the acceleration of gravity.

It is assumed that the ground reaction forces for the corresponding left and right wheels are equal. One can notice that the robot body pitch angle Θ (the angle of body rotation about ${}^{R}y$ axis) is generally not equal to zero as a result of different sinkage of the front and the rear robot wheels, because of an uneven ground reaction forces distribution. As a result the gravitational acceleration vector in the robot coordinate system, in general case, is equal to ${}^{R}\mathbf{g} = [{}^{R}g_x,\, {}^{R}g_y,\, {}^{R}g_z]^T$ and its application point is at the robot mass center of position described by the vector ${}^{R}\mathbf{r}_{CM} = [{}^{R}x_{CM},\, {}^{R}y_{CM},\, {}^{R}z_{CM}]^T$, and ${}^{R}y_{CM} = 0$.

The vectors of gravitational acceleration, forces and moments of force should be transformed from the absolute coordinate system {*O*} to the robot coordinate system {*R*} using multiplication by the rotation matrix in the form:

$$ {}^{R}_{O}\mathbf{R} = \begin{bmatrix} \cos\Theta & 0 & -\sin\Theta \\ 0 & 1 & 0 \\ \sin\Theta & 0 & \cos\Theta \end{bmatrix}. \tag{19} $$

The dynamic equations of motion in the robot coordinate system have the form:

$$ m_R\, {}^{R}a_{CMx} = \sum_{i=1}^{4} {}^{R}F_{Aix} + m_R\, g \sin\Theta = 2{}^{R}F_{Afx} + 2{}^{R}F_{Abx} + m_R\, g \sin\Theta, \tag{20} $$

$$ m_R\, {}^{R}a_{CMz} = \sum_{i=1}^{4} {}^{R}F_{Aiz} - m_R\, g \cos\Theta = 2{}^{R}F_{Afz} + 2{}^{R}F_{Abz} - m_R\, g \cos\Theta, \tag{21} $$

$$ \begin{aligned} I_{Ry}\, \ddot{\Theta} &= -\sum_{i=1}^{4} {}^{R}F_{Aix}\, {}^{R}z_{CM} - \sum_{i=1}^{4} {}^{R}F_{Aiz}\, {}^{R}x_i = \\ &= -2({}^{R}F_{Afx} + {}^{R}F_{Abx})\, {}^{R}z_{CM} - 2{}^{R}F_{Afz}\, {}^{R}x_f - 2{}^{R}F_{Abz}\, {}^{R}x_b, \end{aligned} \tag{22} $$

where: ${}^{R}x_i = \{{}^{R}x_f, {}^{R}x_b\}$, ${}^{R}x_f = L/2 - {}^{R}x_{CM}$, ${}^{R}x_b = -L/2 - {}^{R}x_{CM}$, ${}^{R}x_{CM}$ and ${}^{R}z_{CM}$ – coordinates of mass center of the robot in {*R*} coordinate system, I_{Ry} – mass moment of inertia about the axis parallel to ${}^{R}y$ and passing through the mass center of the robot.

Moreover, for each robot wheel it is then possible to write the dynamic equation of motion associated with wheel spin:

$$ I_{Wiy}\, \ddot{\theta}_i = T_i + M_{\omega i}, \tag{23} $$

where: I_{Wiy} – mass moment of inertia of the wheel about its spin axis, $\varepsilon_i = \ddot{\theta}_i$ – angular acceleration of spin, T_i – driving torque.

After taking into account the above relationships, it is possible to determine the values of robot linear accelerations in ${}^{R}x$ and ${}^{R}z$ directions, the angular acceleration about ${}^{R}y$ axis and the angular accelerations of wheel spin for driving torques T_i.

3.4. Drive units model and controller

The described model of robot dynamics can be also enhanced with the model of its drive units. It is assumed that: each robot drive unit consists of an identical DC motor, encoder, and transmission system. The DC motor model for the i^{th} drive unit is described by the well-known relationships:

$$ \frac{\mathrm{d}i_i}{\mathrm{d}t} = \left(u_i - k_e n_d \dot{\theta}_i - R_d i_i\right) / L_d, \quad T_i = \eta_d n_d k_m i_i, \tag{24} $$

where: L_d, R_d – respectively inductance and resistance of the rotor, k_e – electromotive force constant, k_m – motor torque coefficient, n_d – gear ratio of the transmission system, u_i – motor voltage input, i_i – rotor current, η_d – efficiency of transmission.

Robot motion is governed by a linear drive controller. Based on the desired and actual angles, and the angular velocities of wheel spin, that is, respectively vectors: $\boldsymbol{\theta}_d = [\theta_{1d}, \theta_{2d}, \theta_{3d}, \theta_{4d}]^T$ and $\boldsymbol{\omega}_d = [\omega_{1d}, \omega_{2d}, \omega_{3d}, \omega_{4d}]^T$ as well as $\boldsymbol{\theta} = [\theta_1, \theta_2, \theta_3, \theta_4]^T$ and $\boldsymbol{\omega} = [\omega_1, \omega_2, \omega_3, \omega_4]^T$, the controller determines the control signal vector $\mathbf{u}$ for the drives of particular wheels.

After assuming that the errors of angles and angular velocities of spin for driven wheels are defined as:

$$ \mathbf{e}_\theta = \boldsymbol{\theta}_d - \boldsymbol{\theta}, \quad \mathbf{e}_\omega = \boldsymbol{\omega}_d - \boldsymbol{\omega}, \tag{25} $$

the control signal $\mathbf{u} = [u_1, u_2, u_3, u_4]^T$ for the motors of driven wheels in (V) can be determined using the control law:

$$ \mathbf{u} = \mathrm{sat}\left(k_P \mathbf{e}_\theta + k_D \mathbf{e}_\omega, \mathbf{u}_{min}, \mathbf{u}_{max}\right), \tag{26} $$

where: sat() – a saturation function, k_P, k_D – the controller gains, and $\mathbf{e}_\theta = [e_{\theta 1}, e_{\theta 2}, e_{\theta 3}, e_{\theta 4}]^T$, $\mathbf{e}_\omega = [e_{\omega 1}, e_{\omega 2}, e_{\omega 3}, e_{\omega 4}]^T$, $\mathbf{u}_{max} = [u_{max}, u_{max}, u_{max}, u_{max}]^T$, $\mathbf{u}_{min} = [0, 0, 0, 0]^T$.

4. Simulation and experimental research

The robot motion simulation studies were conducted in the Matlab/Simulink environment. For the simulations, Runge-Kutta fixed-step solver was chosen with Δt step size. The convergence of solutions with changes of Δt was investigated, which allowed the choice of Δt value as a compromise between results accuracy and computation time.

The robot longitudinal motion is analyzed, that is, the motion in which the robot body and its wheels are in plane motion. It is assumed that the robot motion consists of three phases: accelerating (speeding up) with the maximum acceleration a_{Rmax} over the distance l_r, steady motion with the constant velocity ${}^{O}v_{Rd} = v_{Ru}$, and braking with the maximum acceleration (deceleration) a_{Rmax} over the distance l_h. The robot motion is studied for different maximum values of desired linear velocity v_{Ru}, acceleration a_{Rmax} and total distance length L_p. The considered variants are summarized in Tab. 2.

The following values of the basic design parameters of PIAP GRANITE robot are assumed:

- dimensions: $L = 0.425$ m, $W = 0.59$ m (where: $L = A_1A_3 = = A_2A_4$, $W = A_1A_2 = A_3A_4$, see Fig. 1a), $r_i = r = 0.0965$ m, $b_i = b = 2 \cdot 0.064$ m,

- masses: m_0 = 36.54 kg, m_i = 1.64 kg,
- robot mass center coordinates: ${}^R\mathbf{r}_{CM} = [-0.012, 0, 0.06]^T$ m,
- mass moments of inertia: I_{Wy} = 0.016 kg m^2, I_{Ry} = 0.51 kg m^2,
- tire parameters: $k_{ri} = k_r$ = 40 000 N/m, $c_{ti} = c_t$ = 1 000 Ns/m,
- parameters of the drive units: L_d = 0.0823 mH, R_d = 0.317 Ω, k_e = 0.03 Vs/rad, k_m = 0.03 Nm/A, n_d = 53, η_d = 0.8, u_{max} = 32 V.

Moreover, the dry sand parameters from Tab. 1 are assumed. The constant ratio $k_{\vartheta 2} = const$ was chosen for each of the desired velocities of robot motion so as to obtain agreement of the results of simulation-based and experimental investigations. The acceleration of gravity is assumed g = 9.81 m/s^2. In simulations the following gains of the drive controller are assumed: k_P = 30 V/rad, k_D = 10 Vs/rad and the fixed time step: Δt = 0.05 ms.

The experimental investigations were conducted in a container with sand dedicated for the research. Initially the sand was compacted. The investigations were conducted for the analogous cases of motion as during the simulation studies (Tab. 2). For each variant, three repetitions (trials) were performed. Before each trial, the soil was carefully prepared according to a procedure which included raking and leveling.

5. Results

As a result of the simulation and experimental research, the values of longitudinal slip ratio of the robot in the analyzed variants of motion were obtained as shown in Tab. 3. In the table, the values of the $k_{\vartheta 2}$ ratio used during the simulations are also presented – for those values of coefficients the best agreement with the results of experimental research was achieved. The results shown in the table differ slightly from those reported in [10] because of the robot dynamics model change associated with inclusion of the variable angle of robot body pitch during motion. The best agreement of the experimental and simulation results was obtained in the range of 0.2–0.7 m/s, therefore this range will be taken into account in the further analyses.

Based on the research mentioned above, the relationship between the robot velocity and the ratio of front and rear wheel-terrain contact angles was found.

After assuming that in the case of robot standing still $k_{\vartheta 2}$ = 1, the following relationship that approximates $k_{\vartheta 2}({}^O v_{Rd})$ dependency in the range ${}^O v_{Rd} \in \langle 0, 0.7 \rangle$ m/s is proposed:

$$k_{\vartheta 2}({}^O v_{Rd}) = \exp(-a_\vartheta \, {}^O v_{Rd}). \tag{27}$$

This relationship for a_ϑ = 4.919 and the obtained values of $k_{\vartheta 2}$ ratio are illustrated in Fig. 3. It can be noticed that the biggest error of approximation is for velocity ${}^O v_{Rd}$ = 0.2 m/s, however for this velocity in experimental investigations the uncertainty of measurement using the inertial measurement unit is the highest.

The described approach enables robot motion simulation on sand, with variable velocity of motion (and the resulting variable angle of wheel-ground contact) taken into account in the proposed model.

Knowing values of the slip ratio λ_R, and assuming that $\lambda_i = \lambda_R$ and that $k_{\vartheta 2} = (b_0 + b_1 |\lambda_R|)$, the relationship $k_{\vartheta 2}(\lambda_R)$ can be represented in the form of graph shown in Fig. 4. During analysis of the obtained results one may notice that during robot motion the earlier discussed relationship is also satisfied:

$$\vartheta_{2i} = (b_0 + b_1 |\lambda_i|)\vartheta_{1i}. \tag{28}$$

Because of its limitations (discussed earlier), this function cannot be used in simulations that involve the proposed model. In Fig. 4, apart from the results from Tab. 3, the linear function $k_{\vartheta 2} = (0.4108 - 0.0173\ \lambda_R)$ which approximates the results is also shown.

For the discussed model, the results of simulation research can only agree with the results of experimental investigations for $k_{\vartheta 2} \geq 0$. From the relationship $k_{\vartheta 2}(\lambda_R)$ it follows that in the analyzed case this condition is satisfied for the longitudinal slip ratio $\lambda_R \leq$ 23.75%. Because from the obtained results of experimental investigations it follows that in the analyzed range of velocities, the longitudinal slip ratio λ_R increases with increasing desired velocity of motion ${}^O v_{Rd}$, the described model can be valid up to a certain maximum velocity only.

In the part of the work which follows, the selected results of simulation and experimental investigations in which the earlier described exponential function $k_{\vartheta 2}({}^O v_{Rd})$ was used are discussed.

The proposed approach allows exact inclusion of the variable velocity of robot motion in the model (in the present case associated with speeding up and braking). However, the results presented below slightly differ from those obtained as a result of the simulation of motion for the constant value of $k_{\vartheta 2}$, because of errors of approximation of the $k_{\vartheta 2}({}^O v_{Rd})$ function.

In Figs. 5-6 the time histories of selected quantities describing robot motion with 0.3 m/s velocity obtained from the simulation and experimental investigations are shown. In the case of experimental investigations, the driving torques were estimated based on the measured current flowing through the motor windings.

From comparison of the obtained results, it follows that in the case of experimental investigations the delay between the robot body longitudinal velocity ${}^{R}v_{Rx}$ and the circumferential velocity v_o is larger than in the case of simulation (cf. Figs. 5a and 6a). This results in the long-lasting large positive value of slip ratio in the initial phase of robot motion (Fig. 6b). One of the causes of this effect may possibly be the rotational flexibility of the tires.

Additionally, in the final phase of robot motion, because of the unsteady time histories of the wheel circumferential velocities and of the body longitudinal velocity, and because of larger uncertainty of velocity measurement using the inertial measurement unit for small velocities of motion, violent oscillations of the calculated slip ratio occur. For this reason, the final parts of the experimental slip ratio plots are excluded from the present analysis.

The obtained time histories of driving torques (cf. Figs. 5c and 6c) are generally similar, however, in the case of experimental investigations visibly greater maximum values of driving torques for the rear wheels occur and a larger difference of torques for the front and rear wheels is noticeable. In the experimental investigations also minor differences in rotation of the left- and right-hand side wheels were noticed which results in small differences of time histories of the driving torques. In Fig. 6c the results for the left-hand side wheels only are shown.

In Figs. 7 and 8 are presented the time histories for analogous quantities as previously, but this time for the 0.7 m/s robot longitudinal velocity. After examining velocity time histories (Figs. 7a and 8a) it can be noticed that this time larger discrepancy between actual velocity and desired velocity occurs (as compared to the 0.3 m/s case). Time required to reach the maximum value is longer, and the maximum value of the actual velocity during the steady motion is visibly smaller than the desired value. By comparing the results, one may notice longitudinal velocity oscillations of relatively low frequency occurring for experimental results and not present in the simulations.

This phenomenon may be associated with several effects like tire elasticity and damping in the circumferential direction, the effect of bulldozing the sand in front of a tire or displacement of sand behind a rotating wheel, and will be subject to further analyses. Driving torques (Figs. 7c and 8c) have similar time histories and maximum values, but during the initial phase of motion, a visibly greater maximum value for the rear wheel was obtained (in Fig. 8c results for the left-hand side wheels are shown). In comparison to the 0.3 m/s case, this time one can notice that during steady motion smaller differences of the maximum values of driving torques occur between the front and rear wheels.

6. Conclusion

In the present work results of simulation and experimental investigations of longitudinal motion on soft ground of the lightweight robot equipped with small diameter wheels are presented. The influence of various desired longitudinal velocities of motion on robot dynamics was investigated. The findings were incorporated into a model of robot dynamics based on the classical terramechanics models of Bekker and Janosi-Hanamoto.

The most significant conclusions from the research can be summarized as follows:

- A $k_{\vartheta 2}({}^{O}v_{Rd})$ function that enables simulation of robot motion on sand with variable velocity and taking into account the change of ϑ_2 wheel-terrain contact angle at changing robot desired velocity was proposed.
- It was noticed that the obtained simulation results are visibly affected by the value of ϑ_2 angle which was calculated based on the ϑ_1 angle by multiplication through the assumed $k_{\vartheta 2}$ ratio.
- For the given velocities of robot motion in the range 0.2-0.7 m/s a good agreement of simulation and experimental results was achieved.

Acknowledgements

The work has been realized as a part of the project entitled “Dynamics modelling of four-wheeled mobile robot and tracking control of its motion with limitation of wheels slip”. The project was financed by the National Science Center of Poland granted on the basis of decision number DEC-2011/03/B/ST7/02532.

References

[1] H.B. Pacejka, Tire and Vehicle Dynamics, 3rd ed., Elsevier, 2012.
[2] M.G. Bekker, Off-the-road locomotion; research and development in terramechanics., University of Michigan Press, Ann Arbor, 1960.
[3] J.Y. Wong, Theory of ground vehicles, 3rd edition, John Wiley, New York, 2001.
[4] P. Dąbek, M. Trojnacki, Requirements for Tire Models of the Lightweight Wheeled Mobile Robots, in: J. Awrejcewicz, K.J. Kaliński, R. Szewczyk, M. Kaliczyńska (Eds.), Mechatron. Ideas Chall. Solut. Appl., Springer International Publishing, 2016: pp. 33–51. http://link.springer.com/chapter/10.1007/978-3-319-26886-6_3 (accessed January 13, 2016).
[5] T. Kobayashi, Y. Fujiwara, J. Yamakawa, N. Yasufuku, K. Omine, Mobility performance of a rigid wheel in low gravity environments, J. Terramechanics. 47 (2010) 261–274.
[6] M. Heverly, J. Matthews, J. Lin, D. Fuller, M. Maimone, J. Biesiadecki, et al., Traverse performance characterization for the mars science laboratory rover, J. Field Robot. 30 (2013) 835–846.
[7] G. Ishigami, A. Miwa, K. Nagatani, K. Yoshida, Terramechanics-based model for steering maneuver of planetary exploration rovers on loose soil, J. Field Robot. 24 (2007) 233–250. doi:10.1002/rob.20187.

[8] K. Iagnemma, S. Dubowsky, Mobile Robots in Rough Terrain: Estimation, Motion Planning, and Control with Application to Planetary Rovers, 2004 edition, Springer, Berlin ; New York, 2004.
[9] M. Salama, V.V. Vantsevich, Tire-terrain normal and longitudinal dynamics and slip power losses of an unmanned ground vehicle, in: ASME Int. Mech. Eng. Congr. Expo. Proc. IMECE, 2013. doi:10.1115/IMECE2013-65946.
[10] Trojnacki M., Dąbek P., Modelling and studies of dynamics of a wheeled mobile robot during longitudinal motion on the soft ground, in: Proceedings of 13th International Conference Dynamical Systems Theory and Applications DSTA'2015, Łódź, December 7-10, 2015, Vol. 2, Awrejcewicz J., Kaźmierczak M., Mrozowski J., Olejnik P., Eds., Dynamical Systems - Mechatronics and Life Sciences, 503-518.
[11] M. Trojnacki, P. Dąbek, Determination of Motion Parameters with Inertial Measurement Units – Part 1: Mathematical Formulation of the Algorithm, in: J. Awrejcewicz, R. Szewczyk, M. Trojnacki, M. Kaliczyńska (Eds.), Mechatron. - Ideas Ind. Appl., Springer International Publishing, 2015: pp. 239–251. http://link.springer.com/chapter/10.1007/978-3-319-10990-9_22 (accessed January 19, 2015).
[12] S. Taheri, C. Sandu, S. Taheri, E. Pinto, D. Gorsich, A technical survey on Terramechanics models for tire–terrain interaction used in modeling and simulation of wheeled vehicles, J. Terramechanics. 57 (2015) 1–22.
[13] Smith, W.C. Modeling of Wheel-Soil Interaction for Small Ground Vehicles Operating on Granular Soil. PhD Thesis, US Army, 2014.
[14] C. Harnisch, B. Lach, R. Jakobs, M. Troulis, O. Nehls, A new tyre-soil interaction model for vehicle simulation on deformable ground, Veh. Syst. Dyn. 43 (2005) 384–394. doi:10.1080/00423110500139981.
[15] Tire friction and rolling resistance coefficients, http://hpwizard.com/tire-friction-coefficient.html (accessed March 30, 2016).

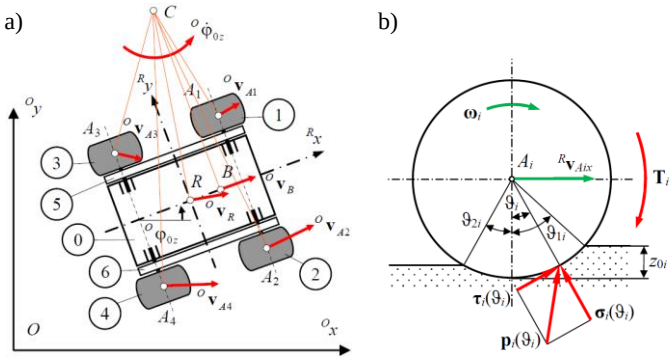

Fig. 1. Kinematic structure of the four-wheeled skid-steered mobile robot (a), modeling of load of wheel moving on deformable ground on assumption of the rigid wheel, after [12] (b).

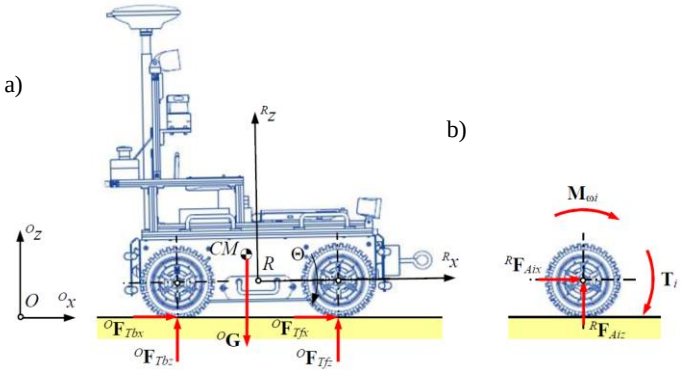

Fig. 2. The forces and moments of force in *Rxz* plane:
a – acting on PIAP GRANITE robot, b – reduced to the center of the wheel (f = 1, 2; b = 3, 4; $L = A_fA_b = 2A_fR = 2A_bR$).

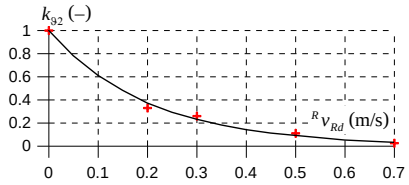

Fig. 3. Relationship between $k_{\vartheta 2}$ ratio and the desired longitudinal velocity of the robot: values of $k_{\vartheta 2}$ ratio (+) and the approximating exponential function (–).

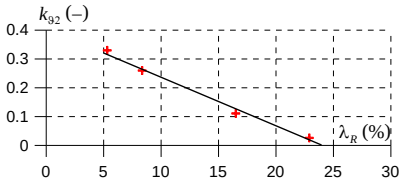

Fig. 4. Relationship between $k_{\vartheta 2}$ ratio and the robot longitudinal slip ratio: values of $k_{\vartheta 2}$ ratio (+) and the approximating polynomial (–).

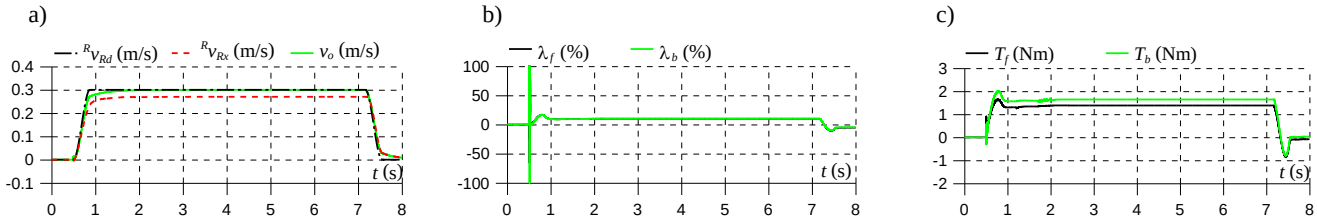

Fig. 5. Time histories obtained in simulation research for the case v_{Ru} = 0.3 m/s.

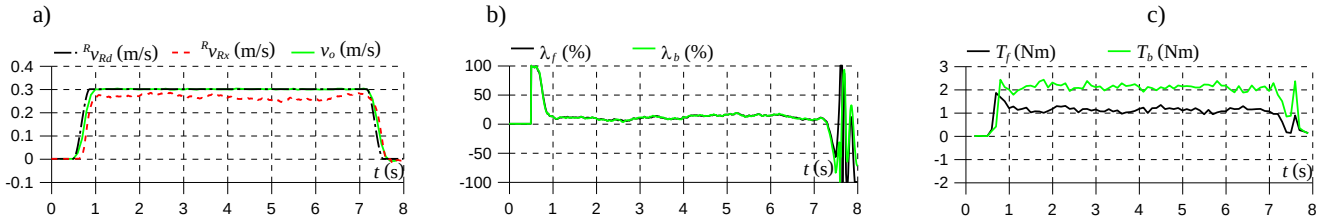

Fig. 6. Time histories obtained in experimental research for the case v_{Ru} = 0.3 m/s.

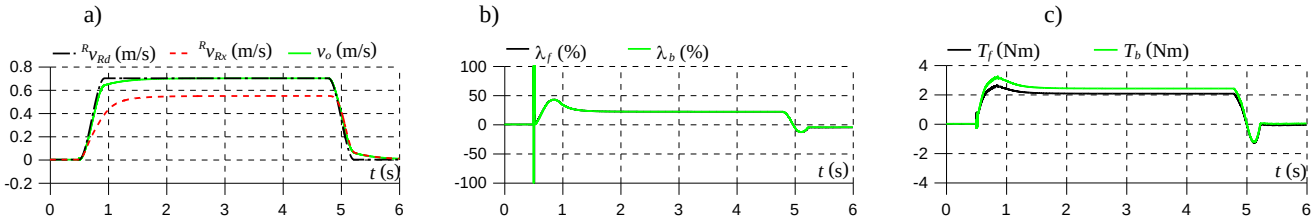

Fig. 7. Time histories obtained in simulation research for the case v_{Ru} = 0.7 m/s.

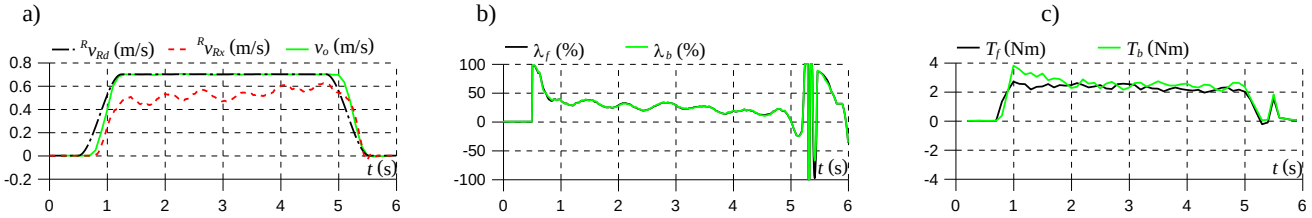

Fig. 8. Time histories obtained in experimental research for the case v_{Ru} = 0.7 m/s.

Table 1. Dry sand characteristic parameters, after [8].

Pressure-sinkage parameters			Shear strength parameters		
n (–)	k_c (kN/m^{n+1})	k_ϕ (kN/m^{n+2})	c (kPa)	ϕ (deg)	K (m)
1.1	0.90	1 523	1.00	30	0.025

Table 2. Motion parameters for the analyzed variants of robot motion.

v_{Ru} (m/s)	0.2	0.3	0.5	0.7
a_{Rmax} (m/s^2)	0.6	1.2	1.2	2.4
L_p (m)	1.0	2.0	2.5	3.0

Table 3. Simulation vs. experimental research results – obtained values of longitudinal slip and $k_{\vartheta 2}$ ratios of the robot in the analyzed variants of motion.

	$^{O}v_{Rd} = v_{Ru}$ (m/s)	0.2	0.3	0.5	0.7
Simulation research	λ_R (%)	5.32	8.55	16.3	23.0
	$k_{\vartheta 2}$ (–)	0.33	0.26	0.111	0.026
Experimental res.	λ_R (%)	5.31	8.35	16.5	22.9